BELLE2-NOTE-PH-2020-054
Draft version 2.5
July 26, 2020

Rediscovery of the $D^0 \to K^0_S K^0_S$ decay with early Belle II data

S. Bharati Das[1], K. Lalwani[1], A. Di Canto[2]

[1] *Malaviya National Institute of Technology Jaipur, Jaipur 302017, India*
[2] *Brookhaven National Laboratory, Upton, New York 11973, USA*

The decay $D^0 \to K^0_S K^0_S$ is among the most interesting modes for the understanding of CP violation in charm decays. In this analysis we aim to “rediscover” this decay and measure its signal yield in early Belle II data.

Contents

Changes with respect to previous versions

v2.5 Implemented comments from reviewers on v2.0.

v2.0 Increased the statistics of the simulation sample; changed to unbinned maximum-likelihood fit; included additional plots as requested by the Charm WG.

1 Introduction

Charge-parity (CP) violation in charm decays has recently been observed by LHCb by measuring the difference between the CP asyemmtries in $D^0 \to K^+K^-$ and $D^0 \to \pi^+\pi^-$ decays [1]. The origin of the observed CP-violation signal is, however, not understood and there is a debate on whether it can be due to physics beyond the standard model [2]. This motivates additional measurements of CP asymmetries in two-pseudoscalar modes to evaluate predictions based on the pattern of $SU(3)_F$ breaking in charm decays [3, 4].

The decay $D^0 \to K^0_S K^0_S$ is a singly Cabibbo-suppressed transition that involves the interference between $c\bar{u} \to s\bar{s}$ and $c\bar{u} \to d\bar{d}$ amplitudes, mediated by the exchange of a W boson at the tree level, that can generate CP asymmetries at the 1% level, even if the Cabibbo-Kobayashi-Maskawa phase is the only source of CP. Moreover, the CP asymmetry is nonvanishing only when $SU(3)_F$ is broken. Both these features make the $D^0 \to K^0_S K^0_S$ mode quite important in the understanding of the origin of CP violation in charm decays [5, 3].

Current experimental measurements of the CP asymmetry in $D^0 \to K^0_S K^0_S$ decays are still limited by the statistical precision, with the best measurement performed by Belle using $921\,\mathrm{fb}^{-1}$ of integrated luminosity: $\mathcal{A}_{CP}(D^0 \to K^0_S K^0_S) = (-0.02 \pm 1.53 \pm 0.02 \pm 0.17)\%$, where the first uncertainty is statistical, the second systematic and the third due to the CP asymmetry of the reference $D^0 \to K^0_S \pi^0$ mode [6].

The goal of this analysis is to "rediscover" the $D^0 \to K^0_S K^0_S$ decay in the early Belle II data. Assuming reconstruction and selection efficiencies similar to those obtained at Belle, we expect to observe a significant yield of about 195 decays in $37.8\,\mathrm{fb}^{-1}$ of Belle II data [6].[1]

The note is structured as follows. The data sample and selection criteria used are presented in section 2 and section 3, respectively. The signal decay yields are determined in section 4 and final results are presented in section 5. The material that is intended to be approved is collected in Appendix A.

2 Data samples

The analysis uses $D^{*+} \to D^0\pi^+$ candidates reconstructed in the data collected by Belle II during experiments 7, 8 and 10 in 2019 and during experiment 12 in 2020. The 2019 data have been processed with `proc11` and, after the good-run list selection, correspond to $9.6\,\mathrm{fb}^{-1}$ of integrated luminosity. The 2020 data are from the prompt processing of `bucket9-12` and, after the good-run list selection, correspond to $28.2\,\mathrm{fb}^{-1}$.

The centrally produced run-dependent (`MC13b_proc11`) generic samples, corresponding to integrated luminosity of $40\,\mathrm{fb}^{-1}$, are used for comparison with data and for understanding of the sample composition. Unless specified, data and simulation samples are processed in the same way, starting with a selection of the signal candidates as described in the following section.

The software version used is `light-2002-ichep`.

[1]Belle observed a total 5399 (4755) signal decays, when requiring $p_{\mathrm{cms}}(D^{*+}) > 2.2\ (2.5)\,\mathrm{GeV}/c$. The estimated 195 decays is based on the yield corresponding to the tighter requirement, since this is what also used in the present analysis.

3 Signal selection

Events with signal decays are first selected by the `hlt_hadron` skim, which requests the presence of at least three good tracks (with transverse momentum $p_{\mathrm{T}} > 0.2\,\mathrm{GeV}/c$ and impact parameters $|d_0| < 2\,\mathrm{cm}$ and $|z_0| < 4\,\mathrm{cm}$) and vetoes events consistent with Bhabha scattering. Candidate $K^0_{\mathrm{S}} \to \pi^+\pi^-$ decays are reconstructed using a merged list of `V0` particles reconstructed by the tracking and pairs of oppositely charged pions combined together offline. Overlapping candidates are removed giving priority to `V0` particles. The K^0_{S} candidates are fit with `TreeFitter` [7]. Only candidates with converged fits and satisfying $0.45 < m(\pi^+\pi^-) < 0.55\,\mathrm{GeV}/c^2$ are retained. Pairs of K^0_{S} candidates are combined to form candidate $D^0 \to K^0_{\mathrm{S}}K^0_{\mathrm{S}}$ decays. The mass of the D^0 candidate, $m(K^0_{\mathrm{S}}K^0_{\mathrm{S}})$, is required to be in the range $[1.70, 2.05]\,\mathrm{GeV}/c^2$. The D^0 mesons are then combined with low-momentum (soft) pions to form a $D^{*+} \to D^0\pi^+$ decay. The soft pion candidates are selected from the list of tracks that are in the CDC acceptance ($17^\circ < \theta < 150^\circ$), are consistent with originating from the interaction point ($|d_r| < 0.5\,\mathrm{cm}$ and $|d_z| < 2\,\mathrm{cm}$), have at least one hit in the CDC. The difference between the D^{*+} and D^0 masses must be $\Delta m < 0.16\,\mathrm{GeV}/c^2$. The D^{*+} candidates are fit using `TreeFitter` by constraining the D^{*+} vertex to be consistent with the measured position of the beams interaction point (IP constraint) and by constraining the masses of the two K^0_{S} candidates to the nominal mass [8]. Only candidates with successful fits and having vertex-fit χ^2 probabilities larger than 10^{-3} are retained for subsequent analysis. The momenta of all final-state particles are updated with the results of the vertex fit. The flight-distance significance of the K^0_{S} candidates, computed by `TreeFitter` as the distance between the K^0_{S} and D^0 vertices divided by its uncertainty, is required to be larger than 10 to suppress peaking backgrounds due to $D^0 \to K^0_{\mathrm{S}}\pi^+\pi^-$ and $D^0 \to \pi^+\pi^-\pi^+\pi^-$ decays (Figure 1). To suppress events where the D^{*+} candidate results from the decay of a beauty meson, the momentum of the D^{*+} in the e^+e^- center-of-mass system is required to exceed $2.5\,\mathrm{GeV}/c$.

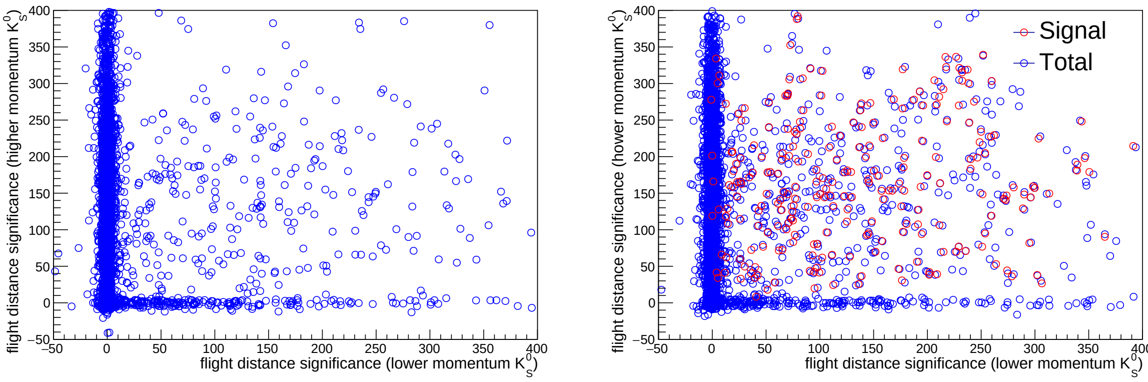

Figure 1: Distribution of the significance of the two K^0_{S} flight distances for $D^0 \to K^0_{\mathrm{S}}K^0_{\mathrm{S}}$ candidates in (left) data and (right) simulation. The simulation plot also shows (in red) the distribution of truth-matched signal candidates. All selection requirements, except for those on the flight-distance significance, are applied. The 1D projections of these distributions are shown in Appendix B.

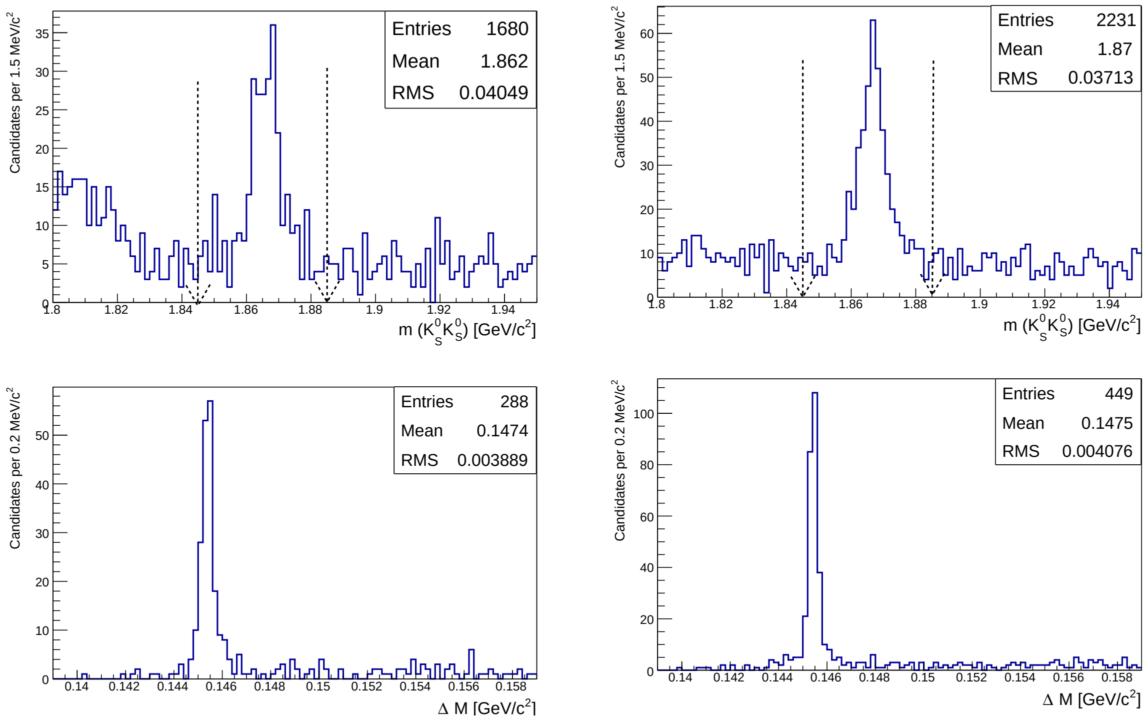

Figure 2: Distribution of (top) $m(K^0_\mathrm{S}K^0_\mathrm{S})$ and (bottom) Δm for $D^0 \to K^0_\mathrm{S}K^0_\mathrm{S}$ candidates in (left) data and (right) simulation. The Δm distribution is only for candidates populating the $m(K^0_\mathrm{S}K^0_\mathrm{S})$ signal region, indicated by the vertical lines, and after the removal of the multiple D^{*+} candidates. The distributions of the D^0 mass for candidates in the Δm signal region is reported in Appendix B.

Figure 2 shows the $m(K^0_\mathrm{S}K^0_\mathrm{S})$ and Δm distributions of the selected candidates in both data and simulation. The shoulder at $m(K^0_\mathrm{S}K^0_\mathrm{S})$ $1.8\,\mathrm{GeV}/c^2$ present in data, but not in simulation, is consistent with a contamination from $D^+_s \to K^0_\mathrm{S}K^0_\mathrm{S}\pi^+$ decays ($\mathcal{B}\ 7.7\times10^{-3}$), in which the charged pion is used as soft pion candidate (see Figure 9 in Appendix B). The Δm distribution is only for candidates populating the $m(K^0_\mathrm{S}K^0_\mathrm{S})$ signal region defined as $1.845 < m(K^0_\mathrm{S}K^0_\mathrm{S}) < 1.885\,\mathrm{GeV}/c^2$. About 2% (2%) of the data (simulated) events in the $m(K^0_\mathrm{S}K^0_\mathrm{S})$ signal region contain multiple D^{*+} candidates. When this happens only the candidate with the largest `TreeFitter` probability is retained.

Figure 3 shows the 2D distribution of the two K^0_S masses for candidates in the $m(K^0_\mathrm{S}K^0_\mathrm{S})$ signal window, passing the best-candidate selection and satisfying $0.1445 < \Delta m < 0.1465\,\mathrm{GeV}/c^2$.

The final list of selection criteria is summarized in Table 1.

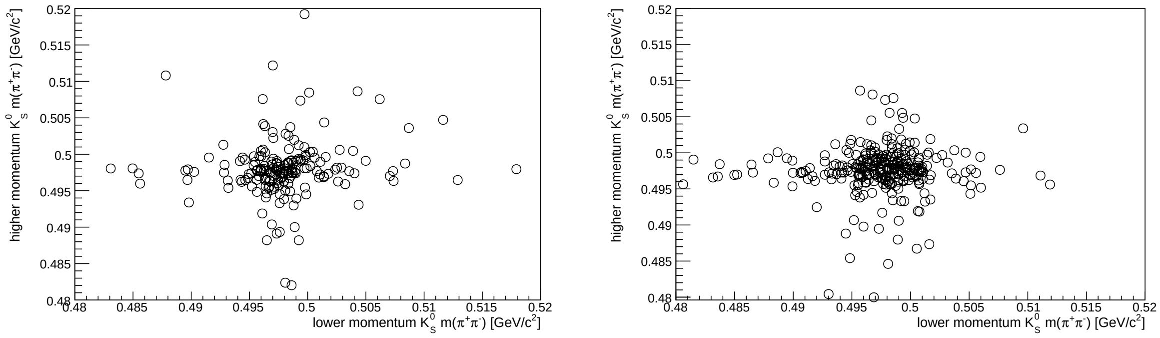

Figure 3: Distribution of the two $m(\pi^+\pi^-)$ for $D^0 \to K_S^0 K_S^0$ candidates in the $m(K_S^0 K_S^0)$ signal window, passing the best-candidate selection and satisfying $0.1445 < \Delta m < 0.1465\,\mathrm{GeV}/c^2$, separately for (left) data and (right) simulation. The $m(\pi^+\pi^-)$ are computed with momenta before `TreeFitter`.

Variable	Criteria
$\lvert d_r\rvert(\pi_s)$	$< 0.5\,\mathrm{cm}$
$\lvert d_z\rvert(\pi_s)$	$< 2\,\mathrm{cm}$
$\theta(\pi_s)$	$[17, 150]^\circ$
# CDC hits (π_s)	> 0
$m(\pi^+\pi^-)$	$[0.45, 0.55]\,\mathrm{GeV}/c^2$
K_S^0 flight-distance significance	> 10
$m(K_S^0 K_S^0)$ (signal region)	$[1.845, 1.885]\,\mathrm{GeV}/c^2$
Δm	$< 0.16\,\mathrm{GeV}/c^2$
$p_{\mathrm{cms}}(D^{*+})$	$> 2.5\,\mathrm{GeV}/c$
`TreeFitter` probability	> 0.001
Best-candidate selection	D^{*+} candidate with largest `TreeFitter` probability

Table 1: Selection criteria. `TreeFitter` is used with an IP constraint and with a K_S^0-mass constraint.

4 Yield fit

The signal yield is determined using an unbinned (and extended) maximum-likelihood fit to the Δm distribution of the candidates in the $m(K_S^0 K_S^0)$ signal region. The fit assumes a signal component described by a Gaussian distribution,

$$\mathrm{pdf}_{\mathrm{sig}}(\Delta m) \propto e^{-\frac{1}{2}\left(\frac{\Delta m-\mu}{\sigma}\right)^2}, \tag{1}$$

and a background component parametrized as

$$\mathrm{pdf}_{\mathrm{bkg}}(\Delta m) \propto (\Delta m - \Delta m_0)^{1/2} + \alpha(\Delta m - \Delta m_0)^{3/2}, \tag{2}$$

where $\Delta m_0 = m_{\pi^+}$ is the kinematic threshold, which is fixed to the known value [8]. The signal and background probability distributions functions are defined only for Δm values larger than the threshold value and are normalized to unity in the fit range, such that in the total fit function,

$$f(\Delta m) = N_{\mathrm{sig}}\, \mathrm{pdf}_{\mathrm{sig}}(\Delta m) + N_{\mathrm{bkg}}\, \mathrm{pdf}_{\mathrm{bkg}}, \tag{3}$$

$N_{\mathrm{sig(bkg)}}$ represents the signal (background) yield. The fit is performed with all shape parameters left free to float.

Results of the fit to the data and simulation samples are reported in Figure 4. The signal yields are estimated to be 177 ± 14 and 256 ± 17 for data and simulation, respectively. The yield in simulation is consistent with the number of truth-matched signal decays of 257 (obtained when requesting `isSignalAcceptMissingGamma` on the D^{*+} candidate). The yield in simulation is larger than the yield in data because the simulation generated the $D^0 \to K_S^0 K_S^0$ decays with a branching fraction of 1.9×10^{-4}, that is $\approx 35\%$ larger than the current world-average value of $(1.41 \pm 0.05) \times 10^{-4}$ [8]. The signal yields per unit luminosity are reported in Table 2, separately for different subsets of the data and for simulation. The simulation yield has been scaled with the ratio 1.41/1.9 to account for the wrong branching fraction used in generation.

Sample (subsample)	Yield per $1\,\mathrm{fb}^{-1}$
Data	4.7 ± 0.4
`proc11`	4.2 ± 0.7
`bucket9-12`	4.9 ± 0.4
Simulation (fit)	4.7 ± 0.3
Simulation (truth-matching)	4.7 ± 0.3

Table 2: Yield per unit luminosity of $D^0 \to K_S^0 K_S^0$ decays for different data and simulation samples. The simulation yield has been scaled with the ratio 1.41/1.9 to account for the wrong branching fraction used in generation.

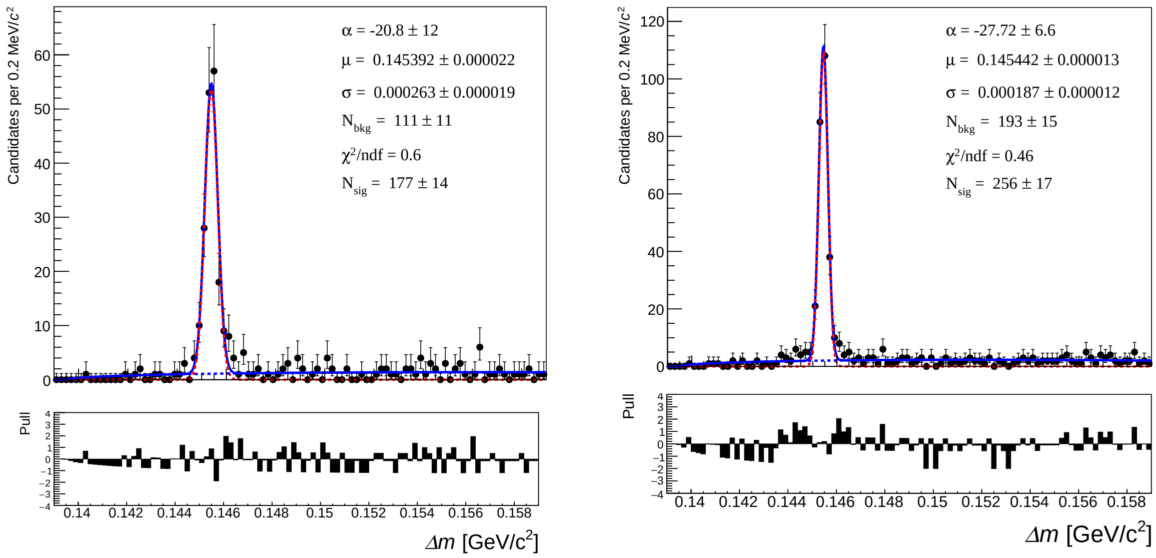

Figure 4: Distribution of Δm for $D^0 \to K^0_S K^0_S$ candidates in (left) data and (right) simulation, with fit projections overlaid. The normalized residuals (pulls) are also shown in the bottom panel of each plot.

5 Results and conclusions

Using the data collected by Belle II during 2019 and the first half of 2020, and corresponding to an integrated luminosity of $37.8\,\mathrm{fb}^{-1}$, we have rediscovered the $D^0 \to K^0_S K^0_S$ decay. The observed yield is

$$N(D^0 \to K^0_S K^0_S) = 177 \pm 14\,, \tag{4}$$

where the uncertainties is only statistical. The yield in unit of integrated luminosity is in agreement with the expectation based on Belle data; the Δm resolution and the purity are, however, better [6].

References

[1] R. Aaij et al., LHCb collaboration, *Observation of CP violation in charm decays*, Phys. Rev. Lett. **122** (2019) 211803, `arXiv:1903.08726 [hep-ex]`.

[2] M. Chala, A. Lenz, A. V. Rusov, and J. Scholtz, *ΔA_{CP} within the Standard Model and beyond*, JHEP **07** (2019) 161, `arXiv:1903.10490 [hep-ph]`.

[3] F. Buccella, A. Paul, and P. Santorelli, *$SU(3)_F$ breaking through final state interactions and CP asymmetries in $D \to PP$ decays*, Phys. Rev. D **99** (2019) 113001, `arXiv:1902.05564 [hep-ph]`.

[4] Y. Grossman and S. Schacht, *The emergence of the $\Delta U = 0$ rule in charm physics*, JHEP **07** (2019) 020, `arXiv:1903.10952 [hep-ph]`.

[5] U. Nierste and S. Schacht, *CP violation in $D^0 \to K^0_S K^0_S$*, Phys. Rev. D **92** (2015) 054036, `arXiv:1508.00074 [hep-ph]`.

[6] N. Dash et al., Belle collaboration, *Search for CP violation and measurement of the branching fraction in the decay $D^0 \to K^0_S K^0_S$*, Phys. Rev. Lett. **119** (2017) 171801, `arXiv:1705.05966 [hep-ex]`.

[7] J.-F. Krohn et al., Belle II analysis software Group, *Global decay chain vertex fitting at B-factories*, `arXiv:1901.11198 [hep-ex]`.

[8] P. A. Zyla et al., Particle Data Group, *Review of particle physics*, Prog. Theor. Exp. Phys. **2020** (2020) 083C01.

A Plots for approval

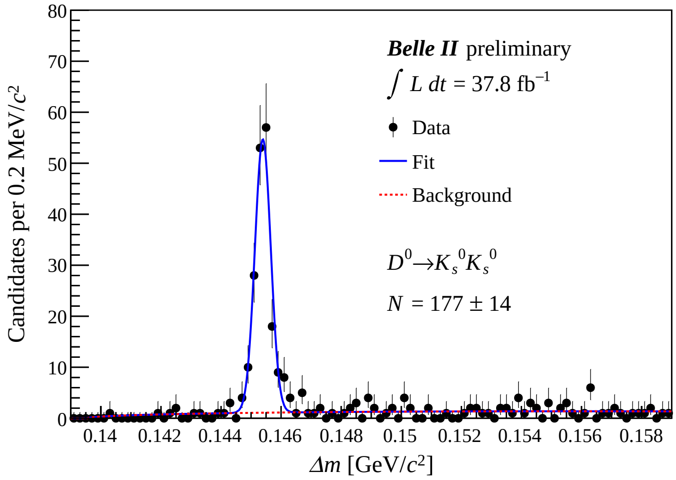

Figure 5: Distribution of the difference between the D^{*+} and D^0 masses (Δm) of $D^{*+} \to D^0(\to K^0_{\rm S}K^0_{\rm S})\pi^+$ candidates reconstructed in the data collected by Belle II during 2019 and the first half of 2020, and corresponding to an integrated luminosity of $37.8\,{\rm fb}^{-1}$, with fit projection overlaid. The Δm distribution is only for candidates populating the signal region $1.845 < m(K^0_{\rm S}K^0_{\rm S}) < 1.885\,{\rm GeV}/c^2$. The signal yield per integrated luminosity is consistent with that observed by Belle; the Δm peak resolution and the signal purity are better than those observed by Belle [6].

B Additional material

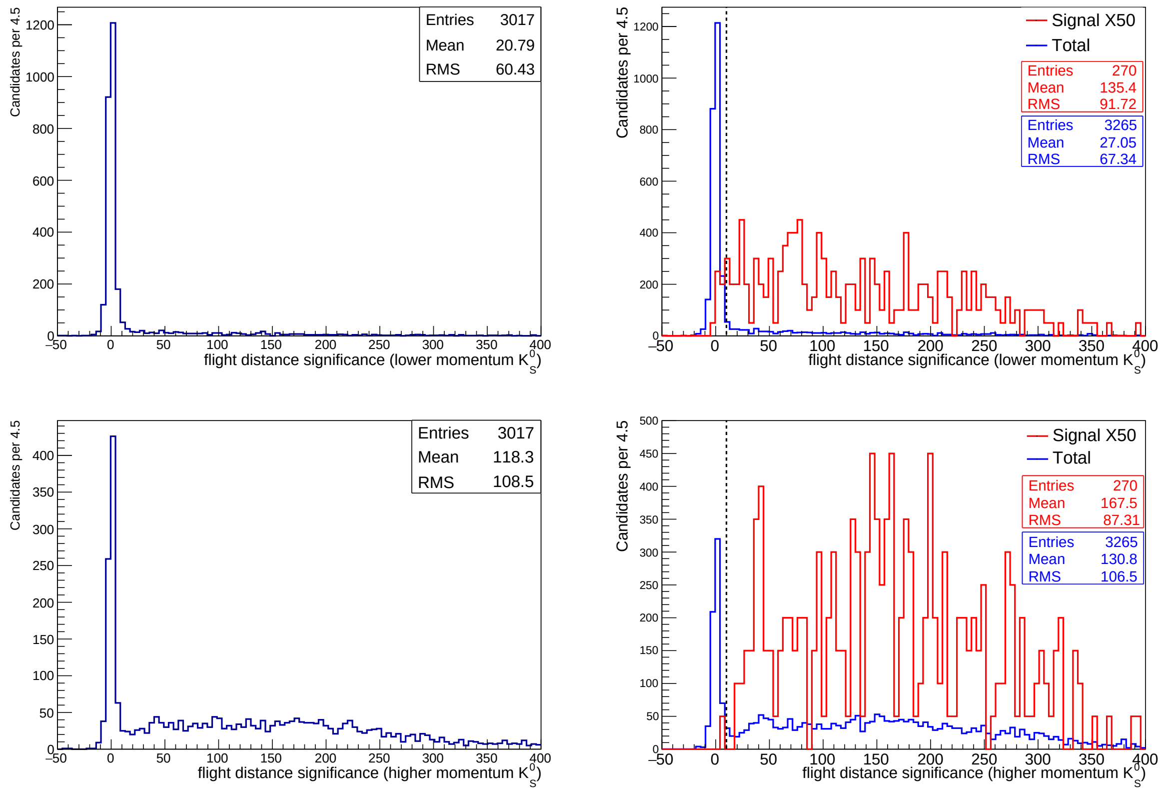

Figure 6: Distribution of the flight-distance significance of the (top) lower-momentum K^0_S and (bottom) higher-momentum K^0_S for $D^0 \to K^0_\mathrm{S} K^0_\mathrm{S}$ candidates in (left) data and (right) simulation. The simulation plot also shows (in red) the distribution of truth-matched signal candidates scaled up by a factor 50. All selection requirements, except for those on the flight-distance significance (shown by the vertical dotted line), are applied.

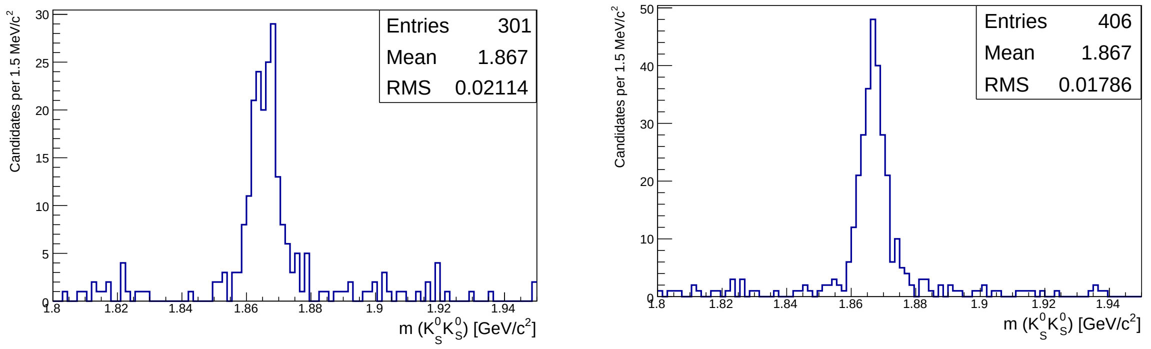

Figure 7: Distribution of $m(K^0_{\rm S}K^0_{\rm S})$ for $D^0 \to K^0_{\rm S}K^0_{\rm S}$ candidates populating the region $0.1445 < \Delta m < 0.1465\,{\rm GeV}/c^2$ in (left) data and (right) simulation. All selection requirements, except for those on the $m(K^0_{\rm S}K^0_{\rm S})$ signal window and on the best candidate, are applied.

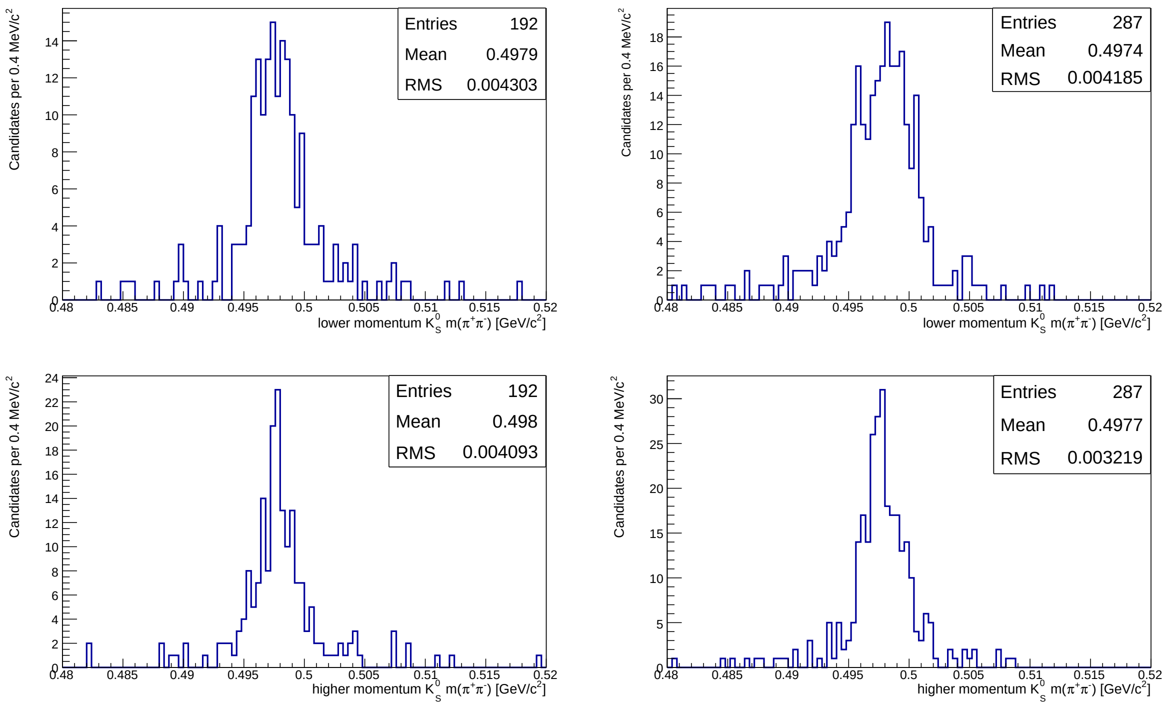

Figure 8: Distribution of $m(\pi^+\pi^-)$ of the (top) lower-momentum $K^0_{\rm S}$ and (bottom) higher-momentum $K^0_{\rm S}$ for $D^0 \to K^0_{\rm S}K^0_{\rm S}$ for candidates satisfying $0.1445 < \Delta m < 0.1465\,{\rm GeV}/c^2$, separately for (left) data and (right) simulation. The dipion masses are computed with momenta before `TreeFitter`.

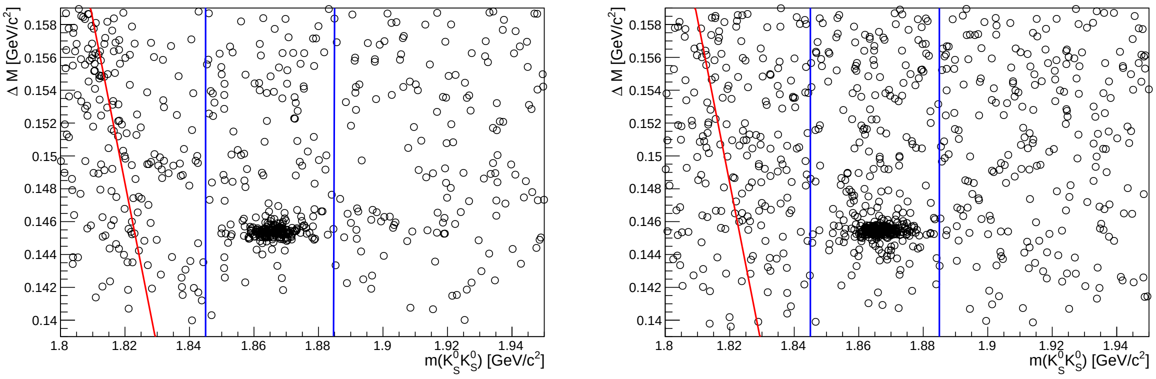

Figure 9: Distribution of Δm vs $m(K^0_S K^0_S)$ for $D^0 \to K^0_S K^0_S$ candidates in (left) data and (right) simulation. All selection requirements, except for those on the $m(K^0_S K^0_S)$ signal window and on the best candidate, are applied. The red line indicates where $D^+_s \to K^0_S K^0_S \pi^+$ decays would contribute and the blue vertical lines indicate the $m(K^0_S K^0_S)$ signal window.

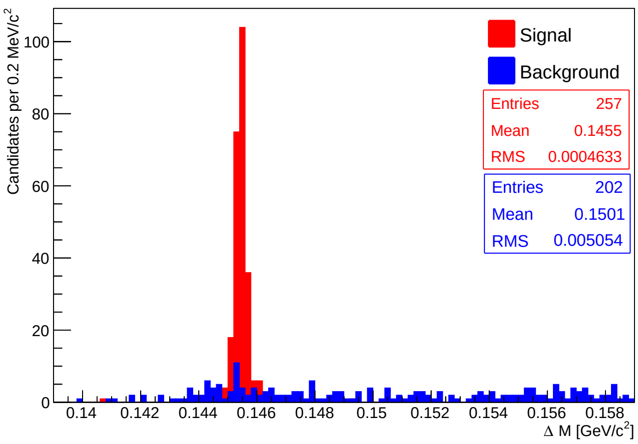

Figure 10: Stacked distribution of truth-matched (red) signal and (blue) background $D^0 \to K^0_S K^0_S$ candidates.

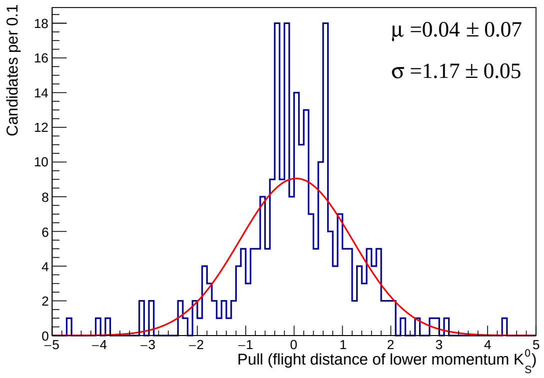

Figure 11: Pull distribution of the flight distances of the two K^0_S for truth-matched $D^0 \to K^0_\mathrm{S} K^0_\mathrm{S}$ signal candidates, with fit projection overlaid. All selection criteria except for those of the flight-distance significance are applied.

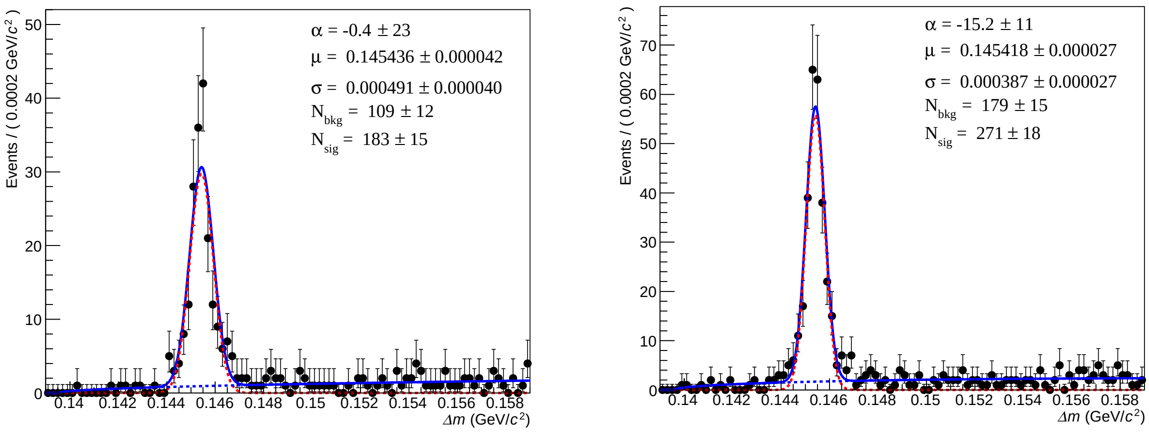

Figure 12: Distribution of Δm computed with masses before `TreeFitter` for $D^0 \to K^0_\mathrm{S} K^0_\mathrm{S}$ candidates in (left) data and (right) simulation, with fit projections overlaid. A comparison with Figure 4 shows that `TreeFitter` improves the peak resolution by a factor of two.